Graphdiyne: An Efficient Hole Transporter for Stable High-Performance Colloidal Quantum Dot Solar Cells

Zhiwen Jin, Mingjian Yuan, Hui Li, Hui Yang, Qing Zhou, Huibiao Liu, Xinzheng Lan, Mengxia Liu, Jizheng Wang, Edward H. Sargent, and Yuliang Li

How to cite TSpace items

UNIVERSITY OF TORONTO
LIBRARIES

www.MaterialsViews.com

ADVANCED
FUNCTIONAL
MATERIALS
www.afm-journal.de

FULL PAPER

Graphdiyne: An Efficient Hole Transporter for Stable High-Performance Colloidal Quantum Dot Solar Cells

Zhiwen Jin, Mingjian Yuan, Hui Li, Hui Yang, Qing Zhou, Huibiao Liu, Xinzheng Lan, Mengxia Liu, Jizheng Wang,* Edward H. Sargent,* and Yuliang Li*

Graphdiyne, a novel large π-conjugated carbon hole transporting material, is employed as anode buffer layer in colloidal quantum dots solar cells. Power conversion efficiency is notably enhanced to 10.64% from 9.49% compared to relevant reference devices. Hole transfer from the quantum dot solid active layer to the anode can be appreciably enhanced only by using graphdiyne to lower the work function of the colloidal quantum dot solid. It is found that the all-carbon buffer layer prolongs the carrier lifetime, reducing surface recombination on the previously neglected back side of the photovoltaic device. Remarkably, the device also shows high long-term stability in ambient air. The results demonstrate that graphdiyne may have diverse applications in enhancing optoelectronic devices.

1. Introduction

Colloidal quantum dots (CQDs) are attractive for next-generation photovoltaic devices due to their low material cost, facile solution processing, high air stability, and their quantum-size-effect bandgap tunability.[1–5] The best-performing devices to date have relied on a depleted-heterojunction architecture, wherein a p-type CQD solid and an n-type TiO_2 or ZnO bulk semiconductor come together to produce a built-in field that separates electrons and holes.[6–11] Power conversion efficiencies (PCE) of such colloidal quantum dots solar cells (CQD solar cells) have recently reached above 9%.

Novel device architectures have played a major role in the rapid improvement in power conversion efficiencies. An improved device architecture has recently been proposed by employing two layer of PbS-EDT (PbS: lead sulfide, EDT: 1, 2-ethanedithiol) as hole transporting layer, groups have advanced the certified AM 1.5 solar power conversion efficiencies to 8.55%.[12,13] The PbS-EDT layers formed a junction with PbS-TBAI (TBAI: tetrabutylammonium iodide) layer, adding in a built-in voltage and also efficiently blocking electrons then facilitating hole transport/extraction, leading to improved performance. Moreover, the resultant devices show much better stability compared to conventional CQD solar cells. Furthermore, inserting a cathode buffer layer between TiO_2 (or ZnO) and the PbS active layer has been found to reduce significantly the interfacial trap density and hence reduce carrier recombination velocities, resulting in improved device performance.[14,15] The improved PCE achieved by adding the electron buffer layer provides a feasible strategy for further development of PbS CQD solar cells.

Modification of the interface by introduction of a buffer layer between the CQD active layer and the anode also deserves attention; however, there is little progress along this important avenue. MoO_3 has been previous attempted but offered little in the way of performance benefits;[13,14] further, it was found to be a chief source of instability resulting from the sensitivity of MoO_3 to H_2O and O_2.[16] Here we develop and deploy a novel hole-transporting material, graphdiyne (GD), as the anode buffer layer. We find that it improves device performance greatly and enables stable device operation.

2. Results and Discussion

Graphdiyne (Figure 2a) is a new allotropic form of carbon nanomaterial. It possesses highly π-conjugated structure consisting of sp^2- and sp-hybridized carbons, in a typical 2D configuration.[17–19] GD has a rigid carbon network, a natural bandgap and uniformly distributed pores, each of which distinguish it qualitatively from graphene. GD has shown encouraging performance in lithium-ion batteries,[20] catalysis,[21,22] photodetector[23] and advanced-performance perovskite solar cells.[24,25]

We synthesized GD on Cu foil via a cross-coupling reaction. We used hexaethynylbenzene as the precursor, and then scraped graphdiyne from the substrate to obtain the resultant black powder (**Figure 1**a). We dried the material under vacuum at 100 °C for 6 h, after which the powder was readily dispersed in chlorobenzene (0.5 mg mL^{-1}) with the aid of magnetic stirring

Dr. Z. Jin, Dr. H. Li, Dr. H. Yang, Dr. Q. Zhou,
Prof. H. Liu, Prof. J. Wang, Prof. Y. Li
Beijing National Laboratory for Molecular Sciences
Key Laboratory of Organic Solids
Institute of Chemistry
Chinese Academy of Sciences
Beijing 100190, P. R. China
E-mail: jizheng@iccas.ac.cn; ylli@iccas.ac.cn

Dr. M. Yuan, Dr. X. Lan, Dr. M. Liu, Prof. E. H. Sargent
Department of Electrical and Computer Engineering
University of Toronto
Toronto, Ontario M5S 3G4, Canada
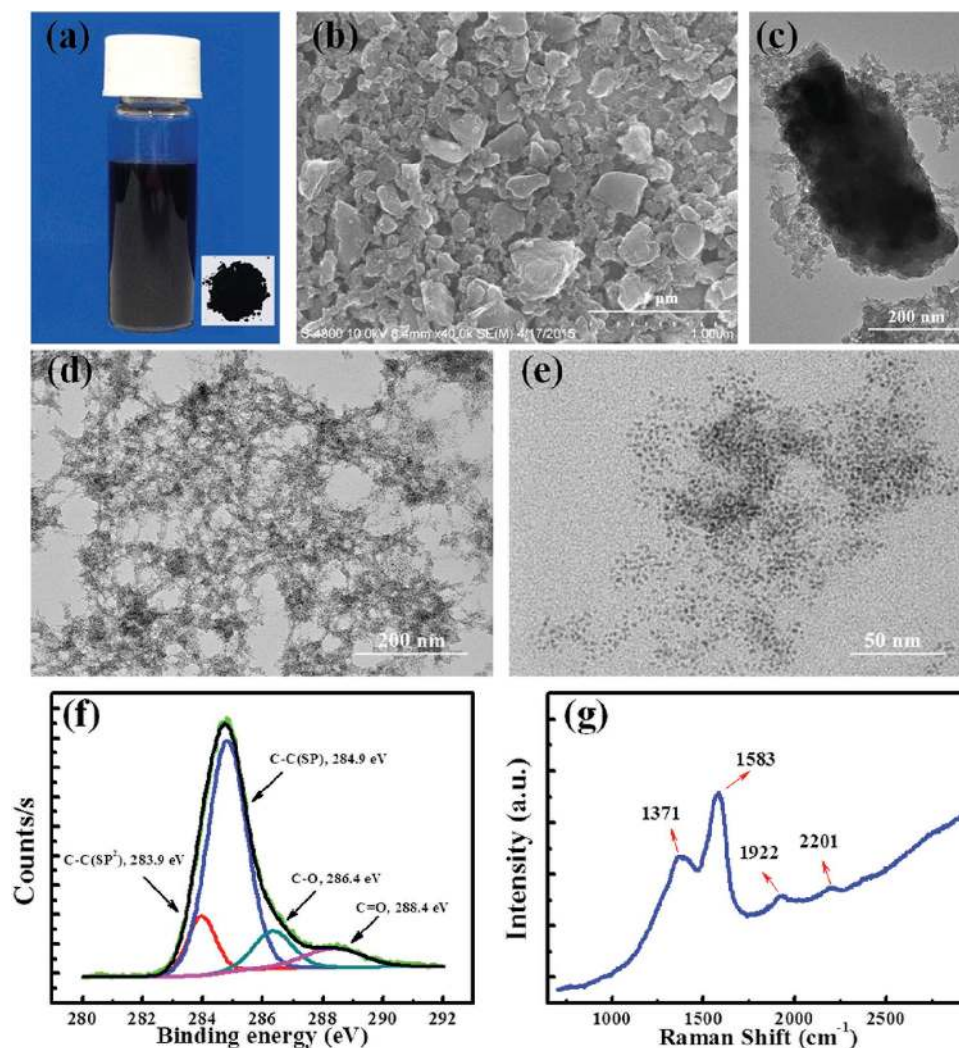E-mail: ted.sargent@utoronto.ca

FULL PAPER

Figure 1. a) Photograph of GD dispersion solution in chlorobenzene. The inset is the GD powder. b) SEM image of GD powder. c) TEM image of GD powder. d) TEM image of dispersed GD. e) High magnification TEM image of dispersed GD. f) XPS spectra of GD with narrow scan for element C. g) Raman spectra of GD.

and ultrasonic dispersion (Figure 1a). We used scanning electron microscopy (SEM) and transmission electron microscopy (TEM) to investigate the morphology of the GD powder. It consisted of flakes several hundred nanometers in size (Figure 1b). Figure 1c shows the TEM image of one GD flake, revealing that flakes consist of many continuously connected small particles. As shown in Figure 1d,e, after being dispersed these particles can be well-separated. It can be clearly seen that these GD particles are actually very uniform with sizes of around 3–5 nm.

X-ray photoelectron spectroscopy (XPS) results shows that GD material (GD powder and GD film) is composed of elemental carbon (Figure 1f). The C 1s peak (at 284.7 eV) is clearly observed for both the powder and the film. After the subtraction of a Shirley background followed by fitting with a mixture function of Lorentzian and Gaussian, the C 1s peak can be deconvoluted into four subpeaks at 283.9, 284.9, 286.4, and 288.4 eV, which can be assigned to a C 1s orbital of C—C (sp^2), C—C (sp), C—O, and C=O, respectively.[26] Here, the O signal

comes from oxygen adsorbed in the pores when the sample was exposed to air (owing to the increased pore size of the GD network induced by the extra alkyne units between the benzene rings).[27] Raman spectroscopy was also used to evaluate the GD powder, which is shown in Figure 1g: the peak at 1371 cm^{-1} is attributed to the breathing vibration of sp^2 carbon domains in aromatic rings.[28] The peak at 1583 cm^{-1} corresponds to the first-order scattering of the E$_{2g}$ mode observed for in-phase stretching vibration sp^2 carbon domains in aromatic rings.[29] The peaks at 1922 and 2201 cm^{-1} can be attributed to the vibration of conjugated diine links (—C≡C–C≡C—).[17]

To evaluate the application potential of GD in PbS CQD solar cells, an architecture of ITO/ZnO/PbS-TBAI/PbS-EDT/Au (the best-performing previously reported device[12,13]) was used for the reference device. The current density–voltage (J–V) characteristics of the device (with GD layer; **Figure 2**a,b) and the reference device are shown in Figure 2c. Static figures of merit for the PbS CQD solar cells with and without GD anode buffer
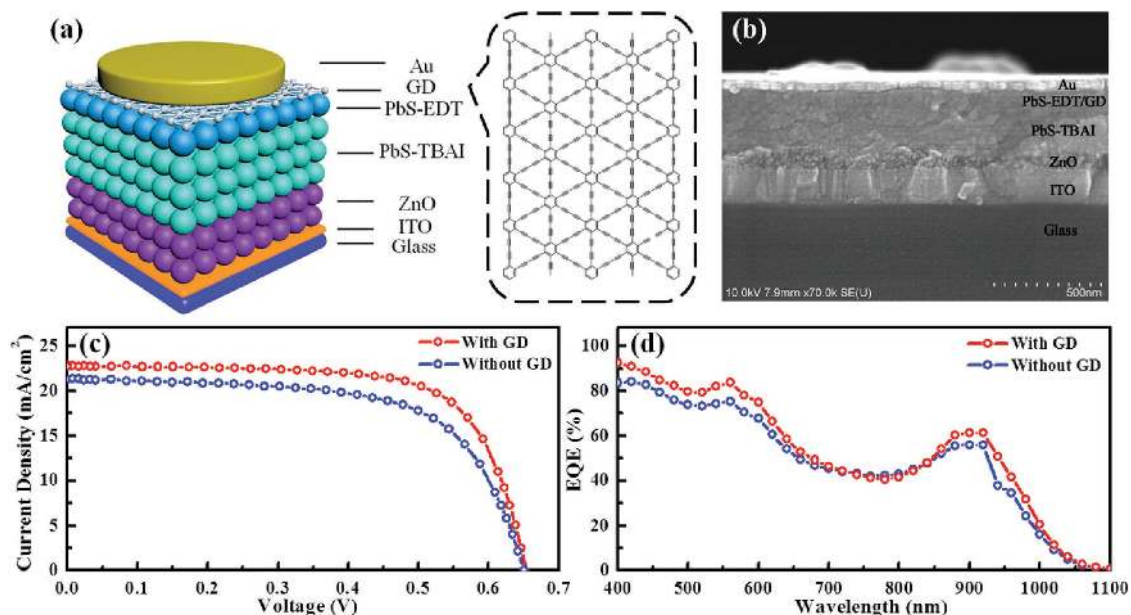
www.MaterialsViews.com

ADVANCED
FUNCTIONAL
MATERIALS
www.afm-journal.de

FULL PAPER

Figure 2. a) Schematic illustration of the PbS CQD solar cells with GD anode buffer layer. b) The cross-sectional SEM image of the device. c) *J–V* characteristics under simulated AM 1.5 G irradiation. d) EQE spectra.

layer are given in **Table 1**. The device exhibits a PCE of 10.64% with a short-circuit current (J_{SC}) of 22.83 mA cm^{-2}, an open-circuit voltage (V_{OC}) of 0.654 V, and a fill factor (FF) of 72.14%, while the reference device displayed a PCE of 9.49% with a J_{SC} of 21.74 mA cm^{-2}, a V_{OC} of 0.650 V, and an FF of 67.34%. External quantum efficiency (EQE) spectra of the devices are shown in Figure 2d, the device exhibits higher EQE than the reference device, which is consistent with its larger J_{SC}.

We sought to investigate the surface chemistry and electronic properties to clarify the mechanistic origins of the beneficial role of the GD layer. The surface morphology and wettability of the GD/PbS film and the PbS film were investigated using atomic force microscopy (AFM) and contact angle measurements. Bare CQD film shows a root-mean-square (RMS) roughness of 3.7 nm (**Figure 3**a), while the GD-treated CQD film has a rougher surface exhibiting RMS value 5.4 nm (Figure 3b). Notably, there exist nanometer-scale islands distributed over the GD/PbS film. As seen in Figure 3c, the CQD film alone shows hydrophobic characteristics with a water contact angle value of 72.2° ± 3.1°, while the GD/CQD film is less hydrophobic with a water contact angle of 50.9° ± 5.3° (Figure 3d). The observation of the small particles and the increased hydrophilicity indicate the existence of GD on the PbS CQDs film. In Figure 3e, the major Raman features of the GD NPs were also observed in the GD/PbS film (the 1371 and 1583 cm^{-1} peaks are clearly seen,

though the 1922 and 2201 cm^{-1} peaks are not seen owing to the very low GD amount on the surface).

Figure 3f gives the absorption spectra of the bare GD film (nominally), PbS film, and GD/PbS film (all on quartz substrates). Although the well-dispersed GD powder exhibits strong absorption, the spin-coated GD film shows no observable absorption, indicating that it is ultrathin and the GD amount is very low. Further investigation found no obvious difference between the absorption on the PbS film and the GD/PbS film, indicating that the involvement of GD particles can rarely influence the absorption of the PbS CQD solar cells. It is thus deduced that the enhanced J_{SC} of the device is not caused by the absorption of the GD thin top layer.

Ultraviolet photoelectron spectroscopy (UPS) is used to determine the valence band edge (E_V) of the GD/PbS film and the PbS film to gain band bending information (Figure 3g). The valence band edge of the GD/PbS film is −5.5 eV, which is higher than that of the PbS film (−5.6 eV) and closer to the work function of Au anode (−5.1 eV). The measured work function (E_F) of the PbS film is 5.1 eV, and that of the GD/PbS film is 5.0 eV. The lower work function of the GD/PbS film indicates that after putting GD on the PbS-EDT film, the vacuum level is pulled down 100 meV. The difference between workfunction E_F and valence band edge E_V remains the same ($E_F − E_V = 0.4$ eV), which means GD actually nearly does not induce any obvious band bending of the CQD layer, and hence does not produce any extra build-in voltage inside the device.[13] The only possible origin of the performance improvement now we can assume would be that GD reduces surface traps (at PbS QD/Au interface) and hence lowers carrier recombination of the device.

In order to gain information about carrier recombination inside the devices, we characterized the devices using impedance spectroscopy (IS). IS is a nondestructive tool that has been widely used in various photovoltaic devices including CQDs.[30–32]

Table 1. Static figures of merit for the PbS CQD solar cells with and without GD anode buffer layer.

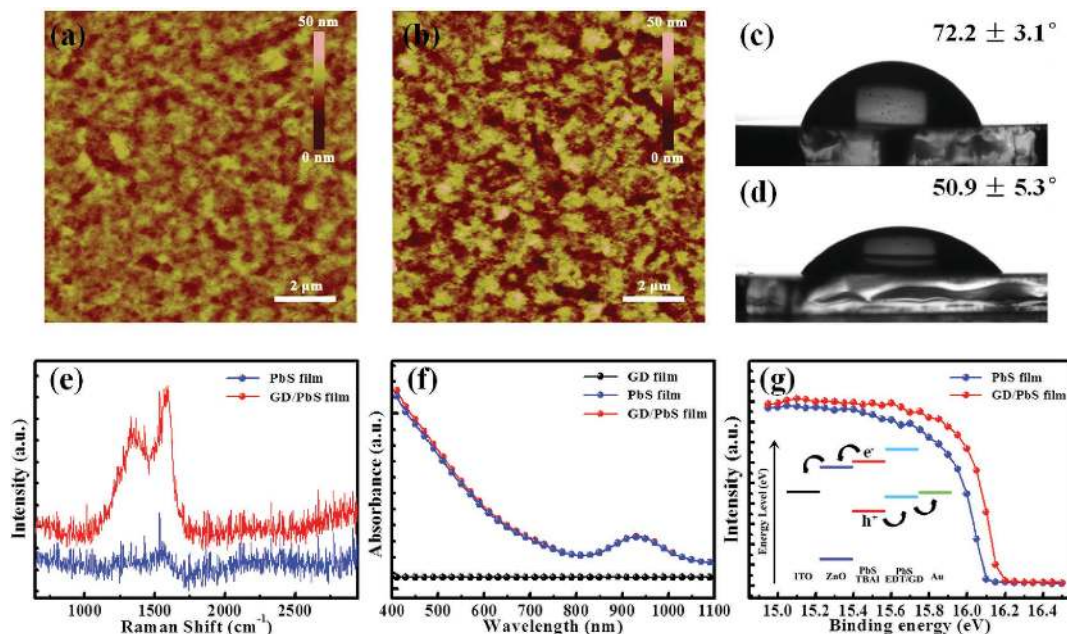|	V_{OC} [V]	J_{SC} [mA cm^{-2}]	FF [%]	PCE [%]
With GD	0.654 ± 0.003	22.83 ± 0.45	72.14 ± 1.42	10.64 ± 0.24
Without GD	0.650 ± 0.004	21.74 ± 0.42	67.34 ± 1.27	9.49 ± 0.27

FULL PAPER

Figure 3. Surface topographic AFM images of a) the PbS film and b) the GD/PbS film. Photographs of water droplet on c) the PbS film and d) the GD/PbS film. e) Raman spectra of the PbS film and the GD/PbS film. f) The absorption spectra of the nominal GD film, the PbS film, and the GD/PbS film. g) UPS spectra of the surface of the PbS film and the GD/PbS film. The energy levels of the device are given as inset.

Figure 4 displays one set of IS data for the devices (in dark (Figure 4a) and under AM 1.5 100 mW cm^{-2} illumination (Figure 4b) at a bias of 0.3 V. From IS data, the effective carrier lifetime can be estimated:[33,34] the peak of the large semicircle in Cole–Cole plot corresponds to a frequency whose reciprocal is the effective carrier lifetime. For the device and the reference device, under illumination the effective carrier lifetime is determined to be 2.4 and 1.9 μs, respectively (the corresponding values in dark are 22.8 and 20.2 μs). The longer carrier lifetime of the device indicates that photogenerated carriers have more time to move toward, and ultimately be collected by the Au anode without suffering recombination. This is consistent with the larger recombination resistance of the device (the diameter of the semicircle), which indicates less carrier recombination inside the device. The longer carrier lifetime and larger recombination resistance should be induced by the improved contact between the PbS-EDT layer and the Au anode.

Transient photovoltage measurement (TPV) was also used to track the recombination rate as a function of V_{OC} (**Figure 5**).[14] The recombination rate R is calculated using the injected carrier density n and the carrier life time τ. It is again seen that the GD device shows a significantly lower recombination rate. The concentration of photogenerated carriers inside the device decreases when GD is present, and the recombination lifetime increases. The GD layer enhances the transport of carriers from CQDs into the electrode, leading to lower steady-state accumulated carrier density in the CQD layer. The TPV results are consistent with the IS observations.

We also evaluated the stability of the devices in time. We stored the devices in ambient air, and tested them periodically. All the parameters, including PCE, FF, J_{SC}, and V_{OC}, are normalized by their corresponding original values at day 0, and then were multiplied by 100%. The results are shown in
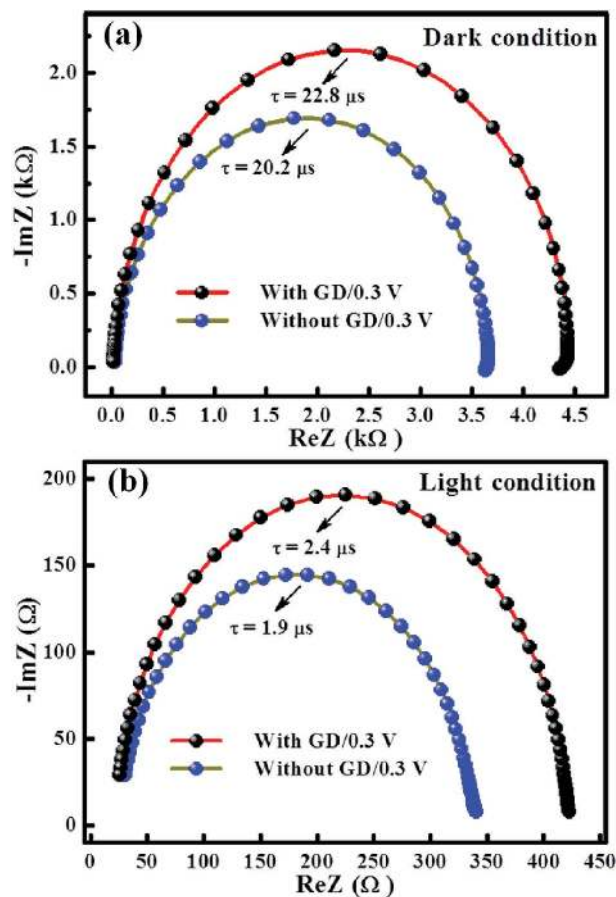

Figure 4. IS results of the devices under a bias of 0.3 V. a) In dark and b) under simulated AM 1.5 illumination.

www.MaterialsViews.com

ADVANCED
FUNCTIONAL
MATERIALS
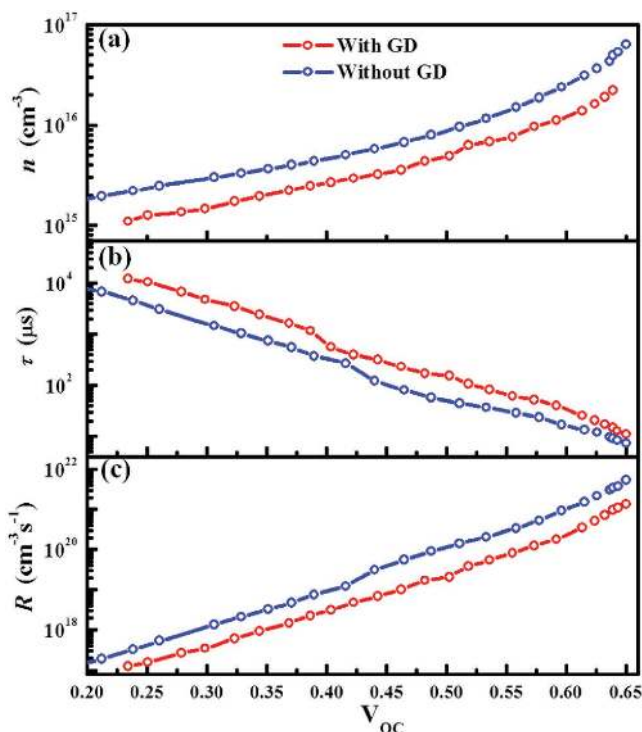www.afm-journal.de

FULL PAPER

Figure 5. Results of transient photovoltage measurements. a) Carrier concentration. b) Carrier lifetime. c) Recombination rate.

Figure 6, it is seen that the device (also the reference device) exhibits very good stability: variations for all the parameters are within 5% over the course of the 120 days.

Figure 6. Stability test. The unencapsulated devices were stored in ambient air during the 120 days. For all the parameters, including PCE, FF, J_{SC}, and V_{OC} are normalized by their corresponding original values at day 0, and then were multiplied by 100%. It is seen that the variations for all the parameters are less than 5% during the 120 days.

3. Conclusion

In conclusion, the novel carbon material, GD is used as anode buffer layer in PbS CQD solar cells. In comparison to the reference device without GD, the PCE is significantly enhanced from 9.49% to 10.64%. IS and TPV measurements indicate GD contributes to increasing carrier lifetime and reducing carrier recombination inside the device, which can be ascribed to the improved interface between the PbS-EDT layer and the Au anode. Notably the device exhibits very good long-term stability. Our work here together with what others already reported hints that the sp^2- and sp-hybridized GD material could have great application in future optoelectronics.

4. Experimental Section

Material Preparation: GD was synthesized on the surface of copper via a cross-coupling reaction using hexaethynylbenzene:[17] the monomer of hexaethynylbenzene was synthesized by addition of tetrabutylammonium fluoride to tetrahydrofuran solution of hexakis[(trimethylsilyl)ethynyl] benzene for 10 min at 8 °C. The GD was successfully grown on the surface of copper foil in the presence of pyridine by a cross-coupling reaction of the monomer of hexaethynylbenzene for 72 h at 60 °C under nitrogen atmosphere. PbS and ZnO quantum dots were synthesized using previously reported methods.[35,36] The concentrations of the PbS dispersed
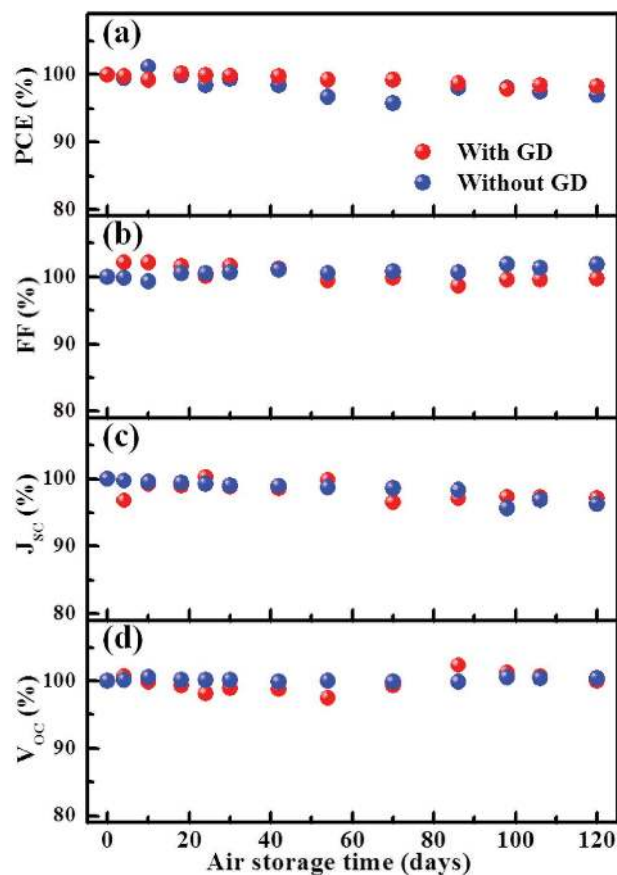
in octane and the ZnO dispersed in chloroform were both 50 mg mL^{-1}. The TBAI solution (10 mg ml^{-1} in methanol) and EDT solution (0.02 vol% in acetonitrile) were stirred rigorously for ≈24 h. The GD solution was prepared by dispersing GD powder in chlorobenzene at a concentration of 0.5 mg mL^{-1}, and then ultrasonicated at 50 °C for 1 week.

Device Fabrication: The photovoltaic devices fabricated process is described as follows: the ZnO layer was fabricated by spin-coating a solution of ZnO quantum dots onto cleaned ITO substrate. Then PbS layers were fabricated by layer-by-layer spin-coating at 2500 rpm for 15 s. To form the PbS-TBAI layer, a TBAI solution was put on the prepared PbS layers for 30 s, followed by two rinse-spin steps with methanol. The formation of the PbS-EDT layer is similar except that EDT solution and acetonitrile were now used (to replace TBAI and methanol). The GD layer was then spin-coated onto the PbS-EDT layer at 2000 rpm for 60 s. All the spin-coating steps were performed under ambient air condition. The films were stored in air overnight and then Au electrodes (100 nm thick) were thermally evaporated onto the films through a shadow mask. Before measurement, the unencapsulated devices were stored in air for another day.

Characterization: The device cross-sectional image was characterized by SEM (Hitachi S-4800) and the GD was characterized by TEM (JEOL JEM-2011). The AFM images were acquired using a Veeco NanoScope IV with a silicon cantilever in tapping mode. The XPS measurements were performed in a Kratos Ultra Spectrometer (a base pressure of 1 × 10^{-9} Torr) using monochromatized Al Kα X-ray photons ($h\upsilon = 1486.6$ eV) discharge lamp. The UPS analysis was performed in a KRATOS ULTRA

FULL PAPER

AXIS DLD photoelectron spectroscopy system with an unfiltered He I (21.22 eV) gas-discharge lamp. Raman spectroscopy measurement was taken using a LabRAM HR800 (Horiba Jobin Yvon) with the excitation energy of 2.62 eV (473 nm). Contact angles were measured on an OCA20 machine (Data-physics, Germany). The average value was obtained from three measurements per sample. Absorption spectra were recorded using JASCO V-570 spectrophotometer.

J–V Characterization and EQE: The steady-state open-circuit voltage, V_{OC}, was first measured using the Keithley 2400 by fixing the current to zero and sampling the voltage at multiple time points. The steady-state short-circuit current, J_{SC}, was measured by setting the bias voltage to zero and sampling the current at multiple time points. Instantaneous *J–V* curves were then measured with a scanning rate of 0.02 V s^{-1}. The steady-state power conversion efficiency, PCE, was measured by setting the bias voltage to the estimated V_{MPP}. Under the bias of V_{MPP}, the current density value was sampled during 15 s to obtain J_{MPP}. The PCE was finally obtained as the product of V_{MPP} and J_{MPP}. The active area was determined by the aperture before the solar cell to avoid overestimating the photocurrent. Through this aperture (area 0.049 cm^2) illumination intensity was calibrated using a Melles–Griot broadband power meter and set to be 1 sun (100 mW cm^{-2}). The AM1.5 solar power was supplied by a class A (<25% spectral mismatch) solar simulator (Science Tech). The spectral mismatch of the system was characterized using a calibrated reference solar cell (Newport). The accuracy of the power measurement was estimated to be ±5 %. The EQE spectra were collected using Oriel IQE-200 in the atmosphere. Prior to the use of the light, the spectral response and the light intensity were calibrated using a mono-silicon detector produced by the National Renewable Energy Laboratory.

IS Measurements: IS measurements were performed using a Zahner Zennium electrochemical workstation. The impedance spectra were recorded by applying varied AC signal from 1 Hz to 1 MHz. All the AC oscillating amplitudes were set as low as 20 mV (rms) to maintain the linearity of the response.

TPV Measurements: In the photovoltage transient method, a 630 nm diode laser was utilized to modulate the V_{OC} on top of a constant light bias. The pulse duration was set to 1 µs and the repetition rate to 50 Hz. The method has been described in details in ref. [14].

[1] J. Tang, H. Liu, D. Zhitomirsky, S. Hoogland, X. Wang, M. Furukawa, L. Levina, E. H. Sargent, *Nano Lett.* **2012**, *12*, 4889.

[2] A. H. Ip, S. M. Thon, S. Hoogland, O. Voznyy, D. Zhitomirsky, R. Debnath, L. Levina, L. R. Rollny, G. H. Carey, A. Fischer, *Nat. Nanotechnol.* **2012**, *7*, 577.

[3] Z. Ning, O. Voznyy, J. Pan, S. Hoogland, V. Adinolfi, J. Xu, M. Li, A. R. Kirmani, J.-P. Sun, J. Minor, *Nat. Mater.* **2014**, *13*, 822.

[4] Z. Ning, H. Dong, Q. Zhang, O. Voznyy, E. H. Sargent, *ACS Nano* **2014**, *8*, 10321.

[5] D. C. J. Neo, C. Cheng, S. D. Stranks, S. M. Fairclough, J. S. Kim, A. I. Kirkland, J. M. Smith, H. J. Snaith, H. E. Assender, A. A. R. Watt, *Chem. Mater.* **2014**, *26*, 4004.

[6] M. R. Kim, D. Ma, *J. Phys. Chem. Lett* **2014**, *6*, 85.

[7] J. M. Luther, J. Gao, M. T. Lloyd, O. E. Semonin, M. C. Beard, A. J. Nozik, *Adv. Mater.* **2010**, *22*, 3704.

[8] A. G. Pattantyus-Abraham, I. J. Kramer, A. R. Barkhouse, X. Wang, G. Konstantatos, R. Debnath, L. Levina, I. Raabe, M. K. Nazeeruddin, M. Gratzel, *ACS Nano* **2010**, *4*, 3374.

[9] J. Tang, K. W. Kemp, S. Hoogland, K. S. Jeong, H. Liu, L. Levina, M. Furukawa, X. Wang, R. Debnath, D. Cha, *Nat. Mater.* **2011**, *10*, 765.

[10] Z. Ning, D. Zhitomirsky, V. Adinolfi, B. Sutherland, J. Xu, O. Voznyy, P. Maraghechi, X. Lan, S. Hoogland, Y. Ren, E. H. Sargent, *Adv. Mater.* **2013**, *25*, 1719.

[11] A. R. Kirmani, G. H. Carey, M. Abdelsamie, B. Yan, D. Cha, L. R. Rollny, X. Cui, E. H. Sargent, A. Amassian, *Adv. Mater.* **2014**, *26*, 4717.

[12] C.-H. M. Chuang, A. Maurano, R. E. Brandt, G. W. Hwang, J. Jean, T. Buonassisi, V. Bulović, M. G. Bawendi, *Nano Lett.* **2015**, *15*, 3286.

[13] C.-H. M. Chuang, P. R. Brown, V. Bulović, M. G. Bawendi, *Nat. Mater.* **2014**, *13*, 796.

[14] M. Yuan, O. Voznyy, D. Zhitomirsky, P. Kanjanaboos, E. H. Sargent, *Adv. Mater.* **2014**, *27*, 917.

[15] G.-H. Kim, F. P. García de Arquer, Y. J. Yoon, X. Lan, M. Liu, O. Voznyy, Z. Yang, F. Fan, A. H. Ip, P. Kanjanaboos, *Nano Lett.* **2015**, *15*, 7691.

[16] Irfan, H. Ding, Y. Gao, C. Small, D. Y. Kim, J. Subbiah, F. So, *Appl. Phys. Lett.* **2010**, *96*, 243307.

[17] G. Li, Y. Li, H. Liu, Y. Guo, Y. Li, D. Zhu, *Chem. Commun.* **2010**, *46*, 3256.

[18] Y. Li, L. Xu, H. Liu, Y. Li, *Chem. Soc. Rev.* **2014**, *43*, 2572.

[19] X. Qian, H. Liu, C. Huang, S. Chen, L. Zhang, Y. Li, J. Wang, Y. Li, *Sci. Rep.* **2015**, *5*, 7756.

[20] C. Huang, S. Zhang, H. Liu, Y. Li, G. Cui, Y. Li, *Nano Energy* **2015**, *11*, 481.

[21] R. Liu, H. Liu, Y. Li, Y. Yi, X. Shang, S. Zhang, X. Yu, S. Zhang, H. Cao, G. Zhang, *Nanoscale* **2014**, *6*, 11336.

[22] H. Qi, P. Yu, Y. Wang, G. Han, H. Liu, Y. Yi, Y. Li, L. Mao, *J. Am. Chem. Soc.* **2015**, *137*, 5260.

[23] Z. Jin, Q. Zhou, Y. Chen, P. Mao, H. Li, H. Liu, J. Wang, Y. Li, *Adv. Mater.* **2016**, DOI: 10.1002/adma.201600354.

[24] C. Kuang, G. Tang, T. Jiu, H. Yang, H. Liu, B. Li, W. Luo, X. Li, W. Zhang, F. Lu, *Nano Lett.* **2015**, *15*, 2756.

[25] J. Xiao, J. Shi, H. Liu, Y. Xu, S. Lv, Y. Luo, D. Li, Q. Meng, Y. Li, *Adv. Energy Mater.* **2015**, *5*, 1401943.

[26] H. Estrade-Szwarckopf, *Carbon* **2004**, *42*, 1713.

[27] M. M. Haley, *Pure Appl. Chem.* **2008**, *80*, 519.

[28] A. Ferrari, J. Meyer, V. Scardaci, C. Casiraghi, M. Lazzeri, F. Mauri, S. Piscanec, D. Jiang, K. Novoselov, S. Roth, *Phys. Rev. Lett.* **2006**, *97*, 187401.

[29] F. Tuinstra, J. L. Koenig, *J. Chem. Phys.* **1970**, *53*, 1126.

[30] L. Etgar, T. Moehl, S. Gabriel, S. G. Hickey, A. Eychmüller, M. Grätzel, *ACS Nano* **2012**, *6*, 3092.

[31] S. S. Kalanur, S. Y. Chae, O. S. Joo, *Electrochim. Acta* **2013**, *103*, 91.

[32] J. Bisquert, *Phys. Rev. B* **2008**, *77*, 235203.

[33] B. Qi, Z.-G. Zhang, J. Wang, *Sci. Rep.* **2015**, *5*, 7803.

[34] G. Garcia-Belmonte, A. Munar, E. M. Barea, J. Bisquert, I. Ugarte, R. Pacios, *Org. Electron.* **2008**, *9*, 847.

[35] M. A. Hines, G. D. Scholes, *Adv. Mater.* **2003**, *15*, 1844.

[36] Z. Jin, J. Wang, *J. Mater. Chem. C* **2014**, *2*, 1966.